JOURNAL OF VIROLOGY, Dec. 2007, p. 12927–12935 Vol. 81, No. 23
0022-538X/07/$08.00+0 doi:10.1128/JVI.00931-07

Interaction of Decay-Accelerating Factor with Coxsackievirus B3▽

Susan Hafenstein,[1] Valorie D. Bowman,[1] Paul R. Chipman,[1] Carol M. Bator Kelly,[1] Feng Lin,[2] M. Edward Medof,[2] and Michael G. Rossmann[1]*

Department of Biological Sciences, Purdue University, 915 W. State Street, West Lafayette, Indiana 47907-2054,[1] and Institute of Pathology, Case Western Reserve University, 2085 Adelbert Road, Cleveland, Ohio 44106[2]

Received 1 May 2007/Accepted 24 August 2007

Many entero-, parecho-, and rhinoviruses use immunoglobulin (Ig)-like receptors that bind into the viral canyon and are required to initiate viral uncoating during infection. However, some of these viruses use an alternative or additional receptor that binds outside the canyon. Both the coxsackievirus-adenovirus receptor (CAR), an Ig-like molecule that binds into the viral canyon, and decay-accelerating factor (DAF) have been identified as cellular receptors for coxsackievirus B3 (CVB3). A cryoelectron microscopy reconstruction of a variant of CVB3 complexed with DAF shows full occupancy of the DAF receptor in each of 60 binding sites. The DAF molecule bridges the canyon, blocking the CAR binding site and causing the two receptors to compete with one another. The binding site of DAF on CVB3 differs from the binding site of DAF on the surface of echoviruses, suggesting independent evolutionary processes.

Coxsackieviruses belong to the family *Picornaviridae*, which contains some of the most common viral pathogens of vertebrates (39, 45, 48, 54, 56, 62). Picornaviruses are small, icosahedral, nonenveloped animal viruses. Capsids have 60 copies of each of four viral proteins, VP1, VP2, and VP3 (Fig. 1) and VP4, that form an icosahedral shell ~300 Å in diameter filled with a positive-sense, single-stranded RNA genome. A prominent feature of the capsid surface is a depression around the fivefold axes of symmetry called the "canyon" (41). The results of both genetic and structural studies have shown that the canyon is the site of receptor binding for many of these viruses (2, 9, 19, 32, 43), including coxsackieviruses which utilize the coxsackievirus-adenovirus receptor (CAR) (13). Receptor molecules that bind into the canyon have been found to belong to the immunoglobulin superfamily (43). When these receptor molecules bind into the canyon, they dislodge a "pocket factor" within a pocket immediately below the surface of the canyon whose shape and environment suggest that it might be a lipid (19, 52). The flexible floor of the canyon is depressed into the pocket when receptor binds. In contrast, the roof of the pocket is pushed upwards when occupied by pocket factor. Hence, the receptor molecule and pocket factor have overlapping binding sites, thus competing with each other for binding to the virus. Absence of the hydrophobic pocket factor destabilizes the virus and initiates transition to altered "A" particles (10), a likely prelude to uncoating of the virion, possibly during passage through an endosomal vesicle (31, 59).

Not all receptors of picornaviruses bind in the canyon. A group of minor rhinoviruses bind to very-low-density lipoproteins (16, 30, 61), and some other picornaviruses, including certain coxsackie- and echoviruses, utilize decay-accelerating factor (DAF) (CD55) as a cellular receptor (7, 22, 36, 50). In general, coxsackievirus serotype B2 (CVB2), CVB4, and CVB6 do not bind DAF, whereas CVB1, CVB3, and CVB5 do bind DAF (49), although there are variations in DAF binding within the CVB3 serotype. Passage of CVB3 through human rhabdomyosarcoma (RD) cells, a cell line that is normally resistant to CVB3 infection, gives rise to a variant form of the virus, CVB3-RD. This variant is able to grow well on RD cells while retaining the ability to infect HeLa cells, albeit with less efficiency and by forming smaller plaques. The binding site of DAF on the surfaces of echovirus 7 (EV7) and EV12 crosses the icosahedral twofold axes of symmetry (4, 13, 35). Mutational analysis has shown that two amino acids, residues 2108 and 2151 (residues in VP1, VP2, VP3 and VP4 are numbered sequentially starting with 1001, 2001, 3001, and 4001, respectively), determine the CVB3-RD phenotype in some strains (24). These residues are located near the twofold axes of symmetry (29). However, subsequent work showed that additional surface residues, 1080, 3137, 3184, and 3234, might contribute to defining the CVB3-RD phenotype (51).

DAF is a member of a family of proteins that regulate complement activation by binding to and accelerating the decay of convertases, the central amplification enzymes of the complement cascade (5, 20, 21, 27). As DAF is expressed on virtually all cell surfaces, the host's cells are protected from attack by the host's own immune system. The functional region of DAF consists of four short consensus repeats (SCR1, -2, -3, and -4), each about 60 amino acids long. The four domains rise about 180 Å above the plasma membrane on a serine- and threonine-rich stalk of 94 amino acids, 11 of which are O glycosylated and attached to the plasma membrane by a glycoslphosphatidylinositol anchor. The entire DAF molecule is relatively rigid, forming an extended rod with dimensions of 160 by 50 by 30 Å (25). Each of the SCR domains is folded into a β structure stabilized by disulfide bridges. The solution structures of the SCR2 and -3 domains and the crystal structures of the SCR3 and -4 domains as well as the full-length human DAF have been determined (25, 60, 64).

Structural and genetic studies have shown that closely related viruses have adapted to bind to DAF at different sites on

* Corresponding author. Mailing address: Department of Biological Sciences, Purdue University, 915 W. State Street, West Lafayette, IN 47907-2054. Phone: (765) 494-4911. Fax: (765) 496-1189. E-mail: mr@purdue.edu.

▽ Published ahead of print on 5 September 2007.

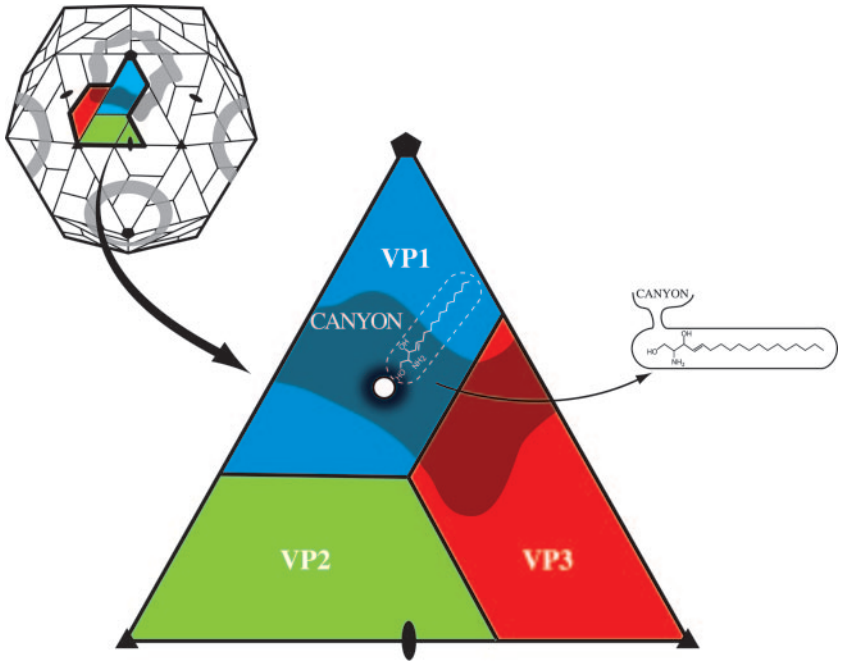

FIG. 1. Diagrammatic view of a picornavirus (top left). A thick black line outlines a protomer, an assembly intermediate. Blue, green, and red correspond to VP1, VP2, and VP3, respectively. One icosahedral asymmetric unit is enlarged (center) to show the location of the canyon and the entrance (white disc) to the hydrophobic binding pocket (white dashed lines) containing the lipid pocket factor. On the right is shown a side view of the pocket, showing the entrance to the pocket from the canyon.

the receptor surface (Table 1) (7, 18, 26, 37, 38, 50, 63). Furthermore, different regions on the same SCR can be utilized by different viruses for attachment (3, 35). Although DAF binding is likely to facilitate viral adsorption and mediate tropism, the availability of DAF receptor molecules on the host is normally not sufficient for CVB3 or EV7 to be able to enter cells (37, 47). Presumably, viral adaptation to bind DAF provides additional advantages. In order to investigate DAF interactions with CVB3, a cryoelectron microscopy (cryoEM) reconstruction of DAF bound to CVB3-RD was made. The binding site of DAF was found to cross the canyon on the viral surface near the "puff" region on VP2 (41) that defines the southern canyon rim.

MATERIALS AND METHODS

Protein and virus production. Human DAF was expressed in *Pichia pastoris* as a C-terminally His_6-tagged protein (14). The DAF construct consisted of the full-length ectodomain, containing SCR1, -2, -3, and -4 (amino acids 1 to 254) but lacking the S/T-rich linker domain and the glycoslphosphatidylinositol anchor.

TABLE 1. Dominant DAF SCR interactions with different related viruses

Virus	DAF interaction at site:			
	SCR1	SCR2	SCR3	SCR4
EV7		X	X	X
EV11			X	
EV12			X	
CVB3		X		
CVB5			X	
CVA21	X	X		
EV70	X			

The ectodomain of CAR protein (D1D2) used in the plaque reduction assays was kindly provided by Paul Freimuth (Brookhaven National Laboratory) and was produced and purified as described previously (13).

The CVB3 M strain (11) was propagated in HeLa cells and purified as described previously (29). CVB3-RD was propagated in RD cells from an inoculum kindly provided by Jeff Bergelson (University of Pennsylvania). RD cells were brought to confluence in 150-mm-diameter plates at 37°C in Dulbecco minimal Eagle medium (Invitrogen) with 10% fetal bovine serum. The cells were rinsed with phosphate-buffered saline (PBS), followed by the addition of 5 ml of CVB3-RD stock inoculum diluted in Dulbecco minimal Eagle medium per dish, for a multiplicity of infection of 1 to 5. After incubation at 37° for 1 h, 7 ml of fresh medium was added per dish, and infection was allowed to progress for 48 h. Cells were harvested, pooled, and stored at −80°C.

Virus was purified by freezing and thawing the cells three times before adding NP-40 (1%). After homogenization, the preparation was centrifuged at 5,000 rpm for 10 min. $MgCl_2$ (to 5 mM), DNase (0.05 mg ml^{-1}), and sodium dodecyl sulfate (to 0.5%) were added to the supernatant and incubated for 30 min at room temperature. Trypsin was added (0.5 mg ml^{-1}) and incubated for 10 min at 37°C. EDTA (10 mM) and sarcosine (1%) were added, and the pH was adjusted to neutral with NH_4OH. The virus was pelleted through 30% sucrose in 50 mM MES (morpholineethanesulfonic acid) (pH 6.0) by centrifugation at 48,000 rpm for 2 h using a 50.2 Ti rotor. The pellets were resuspended in 50 mM MES, loaded onto 10 to 40% K-tartrate–50 mM MES gradients, and centrifuged at 36,000 rpm for 90 min using an SW41 rotor. The virus bands were collected, diluted in buffer, and pelleted by centrifugation at 48,000 rpm for 90 min using a 50.2 Ti rotor. Pellets were resuspended in buffer to estimate the virus concentration by measuring the absorbance at wavelengths of 260, 280, and 310 nm.

Data collection and cryoEM reconstruction. Full-length DAF molecules were incubated with CVB3-RD at room temperature for 1 h at a ratio of four DAF molecules per potential binding site on the virus (240:1). Small aliquots of this mixture were applied to carbon-coated grids and vitrified in liquid ethane. Electron micrographs were recorded on Kodak SO-163 film by using a Phillips CM300 FEG microscope. Micrographs were digitized with a Zeiss PHODIS microdensitometer at 7-μm intervals. The scans were averaged in boxes of 2 by 2 pixels. The final averaged pixel size was 3.11 Å. Approximately 3,500 particles were selected and corrected for contrast transfer function of the microscope using the program RobEM (http://cryoem.ucsd.edu/programs.shtm). The defocus distance ranged from 1.1 to 4.6 μm. The EM reconstruction processes were

TABLE 2. CryoEM data collection

Virus	No. of micrographs	No. of boxed particles	No. of particles used	Defocus range (μm)	Final resolution (Å)
CVB3	9	994	592	2.8–4.8	27
CVB3-DAF	44	3,285	2,269	1.1–4.6	14

performed using icosahedral averaging with the programs EMPFT and EM3DR (1). The cryoEM density of native CVB3 was used as an initial starting structure. The final resolution was estimated by using maps of the reconstructed cryoEM density representing the viral capsid between radii 75 and 160 Å and then determining where the Fourier shell correlation fell below 0.5 using the CUTPIFMAP, FFT, and EMRESOL programs written by Chuan Xiao (http://bilbo.bio.purdue.edu/~viruswww/Rossmann_home/river_programs/). A similar cryoEM reconstruction procedure was used for a reconstruction of the native virus (Table 2).

Difference map and fitting of the DAF structure into the cryoEM densities. The program EMfit (42) was used to calibrate the exact magnification of the cryoEM native CVB3 map by comparing it with a map derived from the X-ray crystallographically determined coordinates of CVB3 (Protein Data Bank [PDB] accession number 1COV). A difference map was calculated by subtracting the native map from the cryoEM map of the CVB3-RD and DAF complex. The SCR2 and -3 fragment was fitted into the cryoEM difference density and refined by using the program EMfit (42) (PDB accession codes for X ray, 1OJV, 1OJW, and 1OJY; PDB accession code for nuclear magnetic resonance, 1NWV). The fitted SCR2 and -3 fragment was then removed from the cryoEM difference density by setting to zero the density within a radius of 4.5 Å of each C_α atom, prior to the independent fitting of SCR1 and SCR4. Residues in the virus/receptor interface were identified as those in CVB3 that had any atoms less than 3.6 Å from any atom in the fitted DAF structure. The buried surface area was calculated using CCP4 programs Areaimol and Surface (Table 3) (6, 8, 23).

Plaque reduction assays. Monolayers of HeLa or RD cells were grown to confluence in six-well 35-mm culture dishes. Virus inoculum was diluted in PBS plus 0.1% (wt/vol) bovine serum albumin to a titer that would allow formation of 50 to 100 plaques. Soluble receptor or an equal volume of PBS plus 0.1% bovine serum albumin was added to the diluted virus and incubated for 1 h at room temperature before being applied to cells. After incubation for 45 min at room temperature to allow virus to attach to cells, the cultures were fed with medium containing 0.8% agar and incubated for 24 to 48 h. The agar overlay was removed, and cells were stained with crystal violet to visualize plaques.

Accession numbers. Accession numbers for data bank deposition are as follows: EMD-1412, cryoEM reconstruction of CVB3 RD strain complexed with DAF; 2QZD, 2QZF, and 2QZH, structures of the ectodomain of the DAF fitted into a cryoEM reconstruction of CVB3 RD strain and DAF complex; EMD-1411, cryoEM reconstruction of CVB3 M strain.

RESULTS AND DISCUSSION

Fitting the DAF structure into the cryoEM complex map. The cryoEM reconstruction of CVB3-RD complexed with full-length DAF (Table 2; Fig. 2) showed that the receptor does not bind into the canyon as does CAR but rather lies across the surface of the virus, crossing over the canyon to interact with the southern rim of the canyon at the "puff" region of VP2 (loop EF, residues 2129 to 2180) (Fig. 2). The cryoEM density corresponding to DAF was approximately equal in magnitude to that of the virion capsid, indicating that nearly all of the 60 possible DAF binding sites were fully occupied. The length and shape of the DAF density corresponded to an extended DAF molecule consisting of four SCR domains. This contrasts with the binding of DAF to the surfaces of EV7 and EV12, which showed only partial occupancy because of low affinity of receptor for virus and steric clashes at the twofold symmetry axes (4, 13, 35).

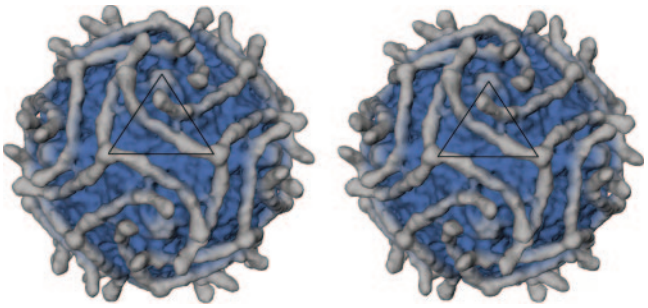

FIG. 2. Surface-rendered cryoEM reconstruction of CVB3-RD complexed with full-length DAF molecules. Density further than a 160-Å radius from the center of the virus is shown in gray. An asymmetric unit is outlined in black. Density corresponding to a full-length DAF molecule with a His tag lies across the asymmetric unit stretching from a threefold axes of symmetry, across and partially blocking the canyon, to the neighboring protomer, rising towards a fivefold vertex. The figure was produced using the program DINO (DINO: Visualizing Structural Biology [2002], http://www.dino3d.org).

Three different crystal structures of DAF (25) generated eight different models with variations of twist and tilt between SCR1 and -2 and between SCR3 and -4. Each of these eight models of full-length DAF was fitted into the DAF difference density using all nonhydrogen atoms (see Materials and Methods for the difference map calculation). The general shape of the DAF molecule, in particular the ~30 to 40° "kink" between SCR1 and SCR2, readily determined the overall orientation. Although the DAF molecule is generally long and cylindrical in shape, the kink or elbow angle modified its shape to permit an accurate orientation of the DAF molecule about its

TABLE 3. Areas of contact between DAF subunits and the virus surface

DAF subunit	Residue no.	Area (Å^2)
SCR1	1–62	0
SCR2	63–127	1,400
SCR3	128–189	558
SCR4	190–252	272

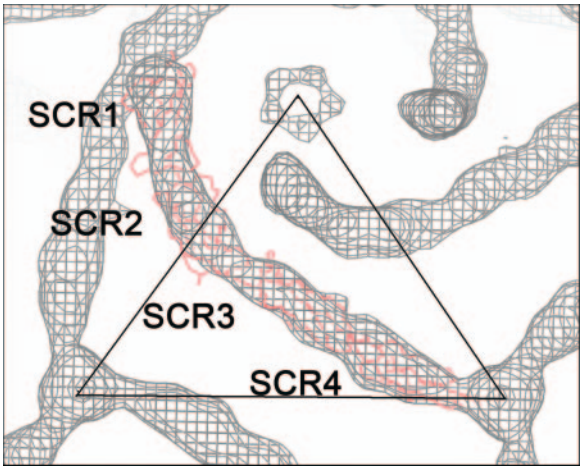

FIG. 3. DAF fitted into the difference density map. The SCR domains are labeled, and the C_α backbone of DAF is shown in red. The figure was produced using the program O (17).

TABLE 4. Results of fitting the structural components of DAF into the cryoEM difference density map

Model[a]	Sumf[b]	Clash (%)[c]	−Den (%)[d]	Orientation (°)[e]			Center (Å)[f]			Sumf as a function of SCR			
				thet1	thet2	thet3	centx	centy	centz	SCR1	SCR2	SCR3	SCR4
10JVa	19.0	0.0	18.5	227.8	29.8	135.2	38.2	6.6	151.1	11.9	19.6	17.8	26.2
10JVb	20.3	0.0	16.6	216.0	43.8	139.8	38.6	6.9	151.4	14.1	20.0	20.6	26.2
10JWa	21.3	0.0	15.8	241.5	22.5	121.5	39.8	8.3	151.8	13.3	23.4	21.7	26.2
10JWb	20.8	0.0	16.1	225.0	32.0	135.0	39.3	7.4	150.9	11.9	24.2	18.7	27.4
10JYa	20.8	0.0	17.1	225.0	13.5	135.0	40.1	8.5	150.8	11.3	24.5	18.3	27.8
10JYb	14.6	8.1	10.8	139.2	16.5	210.0	37.1	16.0	131.5	21.7	17.3	10.2	9.0
10JYc	20.4	1.3	8.6	223.5	11.5	135.0	41.0	9.2	150.9	12.2	20.4	20.0	28.8
10JYd	18.5	0.0	9.0	240.0	347.8	120.0	43.3	9.6	150.3	11.1	19.7	13.0	29.1
XR23	30.6	0.0	10.4	244.8	79.8	132.2	40.0	17.5	150.5	0.0	31.0	30.1	0.0
NMR23	30.0	0.0	2.3	241.5	15.0	120.0	36.2	13.8	149.2	0.0	26.0	33.2	0.0
SCR1	23.7	0.0	1.9	345.0	3.0	15.0	76.4	37.8	148.8	23.7	0.0	0.0	0.0
SCR4	31.7	0.0	2.4	235.5	0.5	120.0	6.4	−31.6	156.6	0.0	0.0	0.0	31.8

[a] Lukacik et al. (25) provide eight different X-ray crystallography structures of DAF from three different crystal forms: two structures of 10JC, designated a and b; two structures from 10JW, designated a and b; and four structures from 10JY, designated a, b, c, and d. XR corresponds to the X-ray crystallographic coordinates for SCR2 and -3 from 10JVa. NMR23 is the first of 42 conformers submitted by Uhrinova et al. (60).
[b] Sumf is defined as the average value of density for all nonhydrogen atomic positions normalized by setting the highest density in the map to 100.
[c] Clash represents the percentage of atoms in the model that have steric clashes with symmetry-related subunits.
[d] −Den provides the percentage of atoms that are positioned in negative density.
[e] Orientation Eulerian angles that rotate the standard orientation of the model into the cryoEM density are given in degrees as described by Rossmann (40).
[f] x, y, and z are the three translational positions of the mass center for the fitted model.

long axis. The asymmetry of the DAF molecule determined the placement of SCR1 closer to a fivefold axis and SCR4 closer to a threefold axis (Fig. 3). However, none of the eight different crystal structures used in their entirety exactly filled the DAF density, indicating that the structure of DAF bound to the surface of the virus had a significantly different tilt and twist between SCR1 and -2 and between SCR3 and -4 than observed in any of the crystal structures. Consequently, a stepwise fitting and refinement operation was used, which first fitted the structure of the central part of the DAF molecule, SCR2 and -3, and subsequently fitted SCR1 and SCR4 separately into the DAF density, by using the EMfit program (40) (Table 4). The best fit of SCR2 and -3 was obtained by using the nuclear magnetic resonance structure (60). The density corresponding to SCR2 and -3 was subtracted from the map, and the full-length structure of DAF (25) was used to initiate the placement of SCR1 and SCR4 into corresponding densities. The position and orientation of SCR1 were refined while restraining the distance between the C terminus of SCR1 and the N terminus of the fitted SCR2 and -3 to be less than 8 Å. Similarly, the SCR4 position and orientation were refined while restraining the N-terminal end of SCR4 to be no more than 8 Å from the C-terminal end of SCR2 and -3. Throughout the stepwise fitting procedure, the full-length DAF structure was used to check that the individual SCRs retained the correct spatial and angular relationships to each other.

Interactions of CVB3-RD and DAF. The crystal structure of CVB3 (CVB3 M strain, PDB accession code 1COV) was placed into the cryoEM density of the CVB3-RD and DAF complex by superimposing the icosahedral symmetry elements. The fitted DAF structure was also placed into the map, and atoms located on the virus surface, as well as atoms in the DAF molecule, were identified if they were within 3.6Å of the two fitted structures (Table 5; Fig. 4). Two loops in the flexible puff region of the CVB3 virus, residues 2134 to 2145 and 2160 to 2168, clashed with the SCR2 of the fitted DAF molecule.

TABLE 5. Fitted DAF residues within 3.6 Å of virus surface residues

CVB3 protein and residue	DAF residue(s)
VP1	
Gln254	Lys76, Gln77, Tyr79, Glu92, Arg101
Tyr255	Lys76
Glu256	Lys76, Glu94, Arg101
Gln264	Glu94, Cys95, Arg101
Pro265	Arg101, Ser104, Leu105
Ser266	Ser104, Leu105, Pro107
Gly267	Leu105, Ser106, Pro107
VP2	
Ala135[a]	Arg100, Arg101, Lys127[b]
Thr136[a]	Gly98, Arg100, Lys127[b]
Leu137[a]	Lys127[b]
Asn138[a]	Pro97, Gly98, Ser176, Val177
Asn139	Pro130, Ser176, Val177
Thr140	Ser176, Val177
Pro159	Pro103
Val160	Arg100, Arg101, Pro103
Ala161[a]	Arg100
Ser162[a]	Gly98, Arg100, Arg101
Gly163[a]	Gly98, Arg100, Lys127[b], Ser128[b]
Ser164[a]	Lys127[b], Ser128[b], Pro130
Asn165[a]	Lys127[b], Ser128[b], Pro130
Lys166[a]	Pro130, Val177
Gln169	Arg100, Arg101
Tyr173	Pro103, Leu195
VP3	
Asn63	Ser104, Leu105, Ser106
Ser232	Glu77, Tyr79, Glu92
Gln233	Gln77, Pro78, Tyr79
Glu234	Lys76, Glu77, Pro78, Tyr79, Ile80, Thr81
VP1[c]	
Asp152	Tyr79, Ile80, Thr81
Lys153	Thr81
Tyr157	Pro78, Tyr79
VP3[c]	
Arg73	Glu207
Asn75	Gly206, Glu207
Glu76	Gln205, Gly206

[a] CVB3 loops 2161–166 and 2135–138 clash with fitted DAF.
[b] Fitted DAF loop 126–128 clashes with CVB3,
[c] Symmetry-related protein.

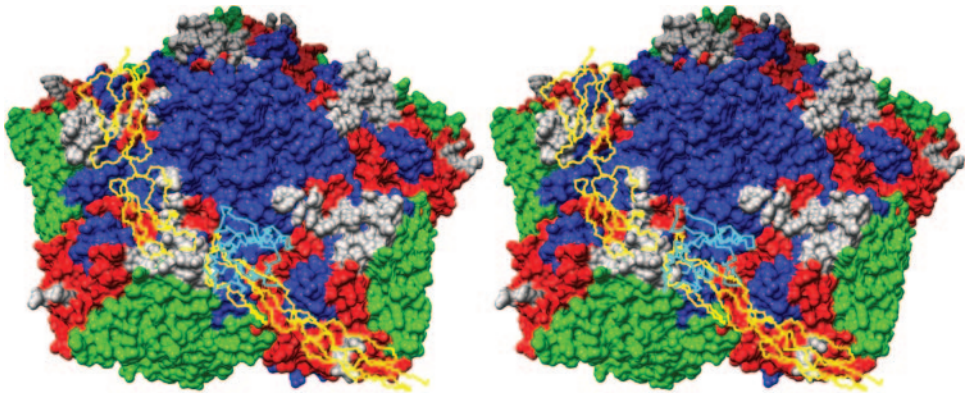

FIG. 4. The surface of CVB3 around a fivefold vertex, with VP1, VP,2, and VP3 in blue, green, and red, respectively. One DAF and one CAR receptor are shown as C_α backbones in yellow and cyan, respectively, where they would be bound to the viral surface. The DAF contact area is shown in white in each of the five protomers. CAR is seen to clash with SCR3 of DAF if both receptors were to bind at the same time to the same icosahedral asymmetric unit of the virus. The stereo figure was produced using Chimera (34, 46).

Presumably these flexible loops alter their structure when forming the complex. Whereas the SCR1 domain of DAF has no interaction with the virus, DAF residues located in SCR2 (residues 76 to 81, 92 to 98, and 101 to 107) were within the contact region. Residues in the SCR2 and -3 junction make a few interactions with the puff, but the main part of SCR3 crosses over the canyon, without entering into the canyon and without making contact with the viral surface. The C terminus of each DAF molecule interacts with two other DAF molecules related by icosahedral threefold symmetry. The site of interaction corresponds to a Ca^{2+} ion, coordinated by Glu3200, as observed in the crystal structure of CVB3 (29). In the complex of CVB3-RD and DAF, this Ca^{2+} ion would also be associated with the carboxy-terminal His_6 nickel binding tag from each of three symmetry-related DAF molecules. Thus, the DAF molecules are effectively tethered to the virus at two sites, namely, at SCR2 and at the carboxy end of SCR4, causing SCR3 to block access to the canyon (Fig. 4).

In agreement with previous affinity measurements and mutational analyses (3, 38), most of the interactions between the receptor and virus occur between SCR2 of DAF and the puff region of the virus. Although the DAF footprints onto the EV7 and EV12 surfaces are similar and involve the puff region on the south side of the canyon, they differ greatly from the footprint of DAF onto CVB3 (Fig. 5 and 6). Furthermore, there is little overlap between the DAF residues involved in binding CVB3 and those that bind EV12 (4) (Fig. 7, left). Most of the DAF residues in the CVB3 contact region are located on the opposite side of DAF than are the residues that interact with convertases, consistent with binding and immunological investigations (12, 20, 21, 53) (Fig. 7, right).

Residues defining the DAF binding sites. Previously, two residues in VP2, Val108 and Ser151, had been identified as necessary for CVB3 infection of RD cells (24). Although Ser2151 maps to the viral surface near the twofold axes of symmetry, Val2108 is located internally on the βD strand of VP2, suggesting that the RD phenotype may not be solely a function of direct receptor interaction. Binding of DAF to the Nancy-new strain of CVB3 has been observed, even though this particular strain had a Ser at position 2151 (RD genotype) and an Asp at position 2108 (wild-type genotype) (51). Furthermore, the amino acid differences reported between Nancy, Nancy-new, and Nancy-RD indicate that there might be some uncertainty as to a common background between different laboratory strains of CVB3 and CVB3-RD, making it difficult to predict which amino acid differences confer DAF binding ability. In contrast to the situation for EV7 and EV12, the structure presented here shows no interaction between DAF and the 2151 surface residue thought to be responsible for the RD phenotype. Possibly the binding site of DAF on CVB3-RD

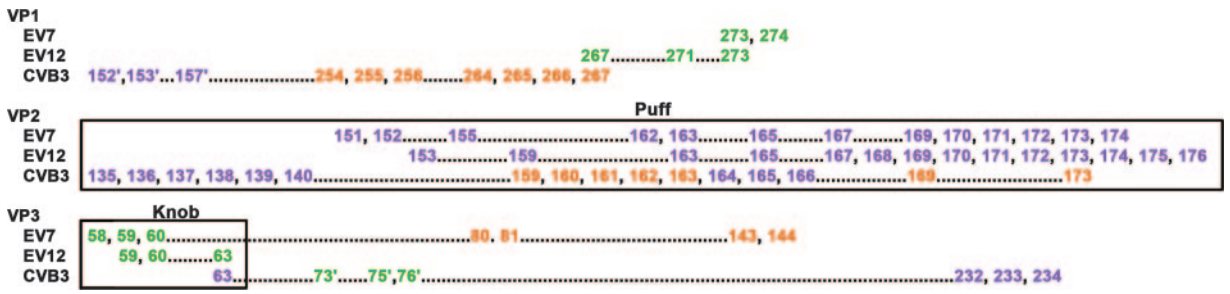

FIG. 5. Echovirus surface residues predicted to interact with DAF, given as equivalent CVB3 residues based on multiple-sequence alignment (CLUSTALW) (57). Virus contact residues are color coded to identify specific DAF SCR interactions, with SCR2 shown in orange, SCR3 in purple, and SCR4 in green. Residues marked with ′ are located in symmetry-related proteins. EV7 and DAF contacts are according to fit (a) in Table 2 in reference 14. EV12 and DAF contacts are from Fig. 6D and E in reference 4.

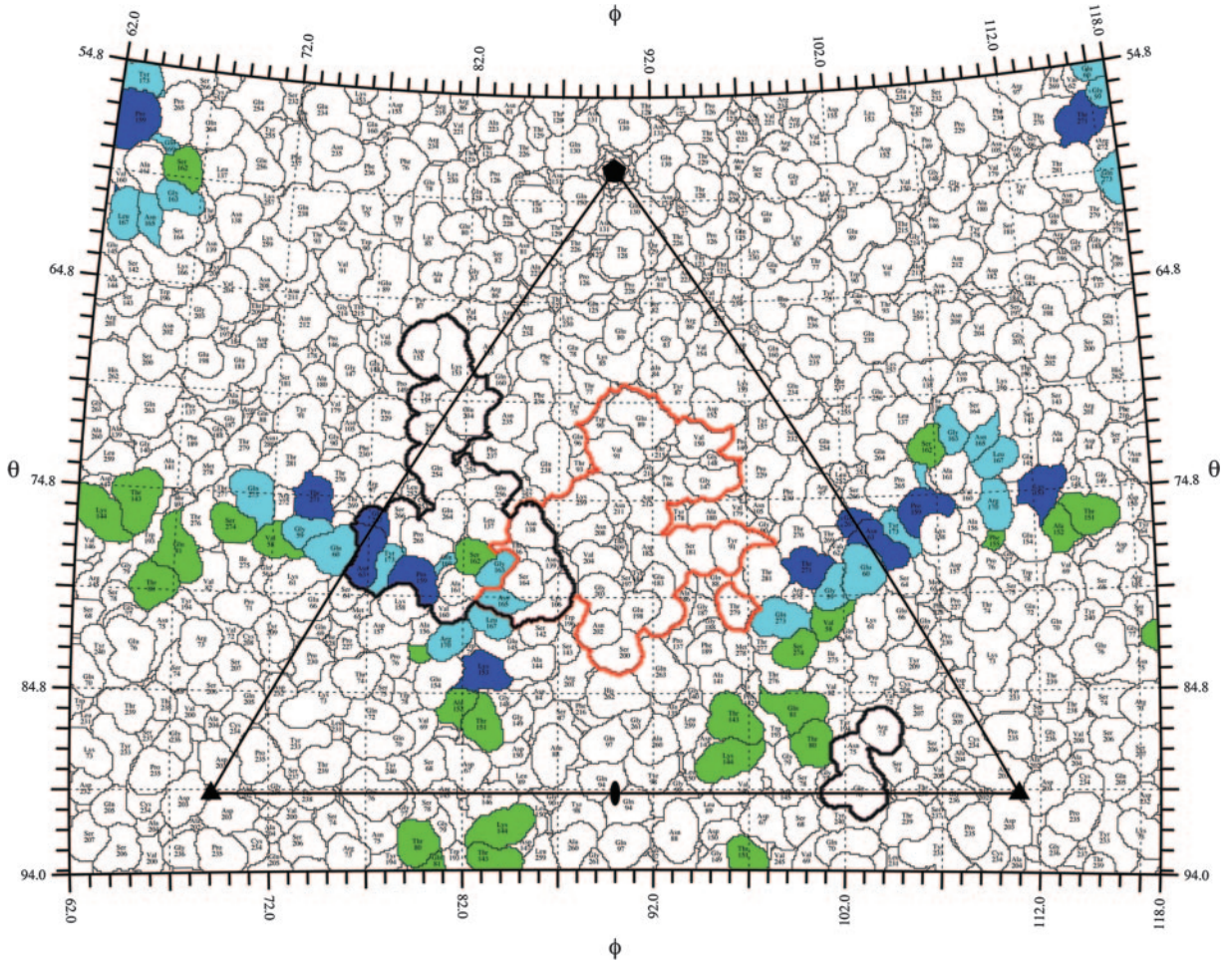

FIG. 6. The viral surface is shown as a stereographic projection where the polar angles θ and φ represent latitude and longitude, respectively (65). The virus surface is represented as a quilt of amino acids (44). The icosahedral asymmetric unit of the virus is indicated by the triangular boundary. The footprint of DAF for echoviruses was plotted using the equivalent CVB3 residues based on multiple-sequence alignment (CLUSTALW) (57). The three viruses have sequence identities of 61% for VP1, 70% for VP2, and 67% for VP3. DAF contact residues for EV7 (14) and EV12 (4) are green and blue, respectively. The overlap between DAF footprints for the two echoviruses is shown in cyan. The DAF and CAR (14) footprints on CVB3 are outlined in black and red, respectively.

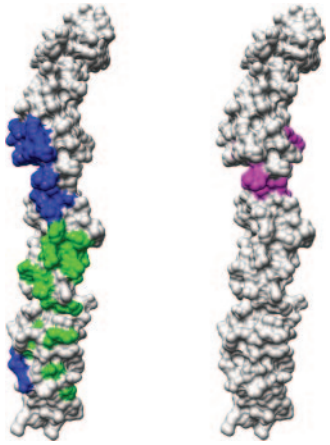

FIG. 7. A surface rendering of the full-length fitted DAF structure, in stereo. (Left) The CVB3 footprint onto DAF (blue) compared to the EV12 footprint onto DAF (green) shows no overlap. (Right) The DAF area predicted to interact with convertases (from reference 20) (magenta) shows no overlap with the echovirus footprint on DAF and a slight overlap of five residues with the CVB3-RD footprint.

has greater affinity to DAF than the binding site observed in the cryoEM studies of echoviruses. This is supported by the much higher occupancy of DAF on CVB3-RD compared to the cryoEM studies of DAF binding to EV7 and EV12. As the two receptor binding sites are mutually exclusive, it would be expected that the site reported here, once established, would be dominant.

Plaque reduction assays. Plaque reduction assays were performed with the uncomplexed wild-type CVB3 (11) and the mutant CVB3-RD, as well as with viruses preincubated with either soluble CAR or DAF (Fig. 8). Reduction of plaques occurred only when wild-type virus was preincubated with soluble CAR and applied to HeLa cells or when mutant virus was preincubated with soluble DAF and applied to RD cells (>90% plaque reduction). In all other combinations, plaque reduction was insignificant. These results can be interpreted by noting that HeLa but not RD cells express CAR, that both types of cells express DAF, and that the structural results show that DAF blocks access to the canyon (Fig. 4). In order to

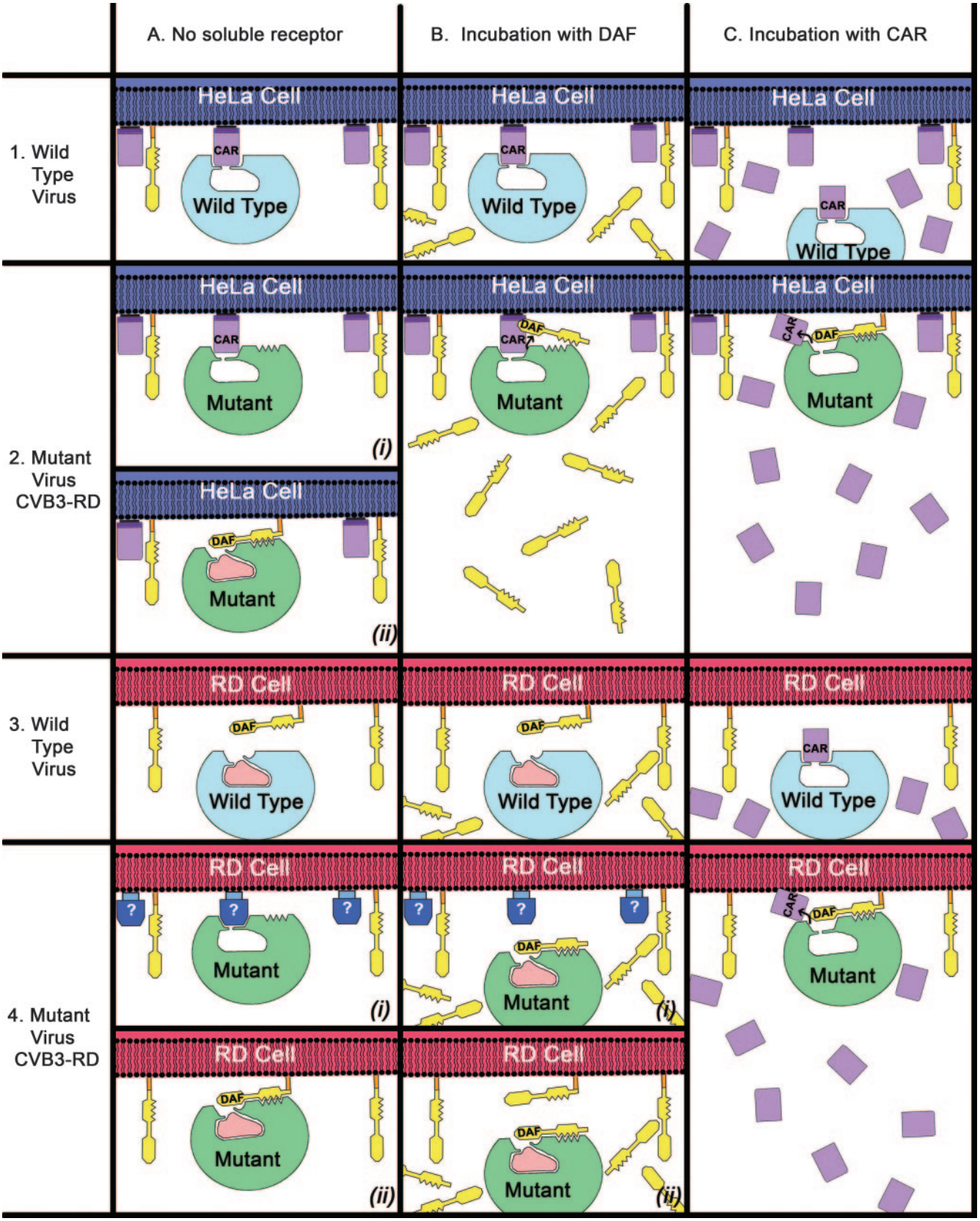

FIG. 8. Interaction of wild-type CVB3 virus (light blue) or mutant CVB3-RD virus (green) with HeLa cells (dark blue) or RD cells (red). HeLa cells express both DAF (yellow) and CAR (lavender) receptors, whereas the RD cells express DAF and possibly an unidentified receptor (blue). The wild-type virus normally contains a pocket factor (pink), which can be displaced by binding of a receptor into the canyon, shown as a U-shaped depression at the top of the virus.

further explain the plaque assay results, it is also necessary to make the following assumptions: adaptation by the mutant virus to bind DAF allows DAF to compete successfully with CAR, and either (i) a canyon-binding receptor molecule displaces the pocket factor or (ii) DAF binding alone is sufficient for the virus to enter and infect cells.

Viral plaque reduction assays indicated that wild-type virus was able to infect HeLa cells but not RD cells (Fig. 8). This is consistent with wild-type virus being able to bind CAR but not DAF. Preincubation of wild-type virus with soluble CAR reduced plaques on HeLa cells, presumably by blocking the CAR binding site. The mutant virus was capable of infecting both HeLa and RD cells. However, compared to wild type, the mutant plaques in HeLa cells were smaller and fewer, suggesting either the mutant virus no longer binds CAR as well as the wild type or that the mutant virus is entering cells in a different, less efficient way. Furthermore, the gained ability of the mutant virus to bind to DAF may be demonstrated by plaque formation in RD cells, although it is unclear whether the virus uses only DAF or an unknown canyon-binding receptor to enter RD cells. Preincubation of the mutant virus with DAF inhibits plaque formation on RD cells but not that on HeLa cells. Either the mutant virus relies on an interaction with DAF to infect RD cells or access to the canyon for a hypothetical unknown canyon-binding receptor was blocked by bound DAF. However, it is possible that CAR molecules on HeLa cells successfully competed with the DAF bound to the surface of the mutant virus, allowing infection. Incubating the mutant virus with CAR caused no reduction in plaque formation on either HeLa cells or RD cells. This lack of inhibition suggests that preincubation of the mutant virus with CAR could have expelled the pocket factor, making the virus susceptible for uncoating. Subsequently, the mutant virus would be able to infect HeLa or RD cells by interacting with DAF.

The above assumption (i) that there might be another molecule on the surface of RD cells that can act as receptor for the mutant CVB3-RD virus would be consistent with the hypothesis that the pocket factor needs to be displaced by a canyon-binding molecule, such as CAR, to initiate uncoating of the virus. It is also consistent with observations that indicate that when CVB3 adapts to use DAF, it retains the ability to bind CAR and remains dependent on a CAR interaction for uncoating (12, 36, 47) and that DAF alone is insufficient to initiate infection (28). Furthermore, CVB3 can bind to at least five different cellular receptors distinct from either DAF or CAR on the surface of human cardiac cells (33). However, the alternative assumption (ii), namely, that DAF alone is sufficient for a successful infection, without the assistance of a canyon-binding molecule to displace the pocket factor, cannot be ruled out. For instance, the minor-group rhinoviruses, which use very-low-density lipoproteins for attachment and infection (16, 61), bind the receptor on an exposed surface outside the canyon (15). Similarly, it has been shown that a DAF-binding strain of echovirus can enter cells by using DAF as a receptor, apparently without forming A particles (55).

Closely related viruses bind different surfaces of DAF to different locations on the virus, suggesting a convergent evolution in the use of DAF that offers some advantage to the virion. Such an advantage may be due to the ubiquitous nature of DAF, which is found on most cell surfaces, including serum-exposed cells that line the lumen through which enteroviruses travel. For instance, DAF is necessary to enter polarized epithelial cells (3), because the initial binding of CVB3 to DAF sets off a cell-signaling cascade which causes transport of the bound virus to the tight junction between cells and allows interaction with CAR molecules that are sequestered there. Similarly, coxsackievirus binding to DAF expressed on pancreatic cells causes recruitment of CAR to the site of the interaction (58), allowing subsequent binding of the CAR and successful infection of the cells.

ACKNOWLEDGMENTS

We thank Sheryl Kelly and Cheryl Towell for help in preparation of the manuscript and Rodney McPhail for assistance with Fig. 1.

Figures 4 and 7 were produced using the UCSF Chimera package from the Computer Graphics Laboratory, University of California, San Francisco (supported by NIH grant P41 RR-01081). The work was supported by National Institutes of Health grants to M.G.R. (AI 11219), to D.E.M. (AI 23598), and to F.L. (HL 077319). S.H. was supported by a National Institutes of Health postdoctoral fellowship (AI 060155).

REFERENCES

1. **Baker, T. S., N. H. Olson, and S. D. Fuller.** 1999. Adding the third dimension to virus life cycles: three-dimensional reconstruction of icosahedral viruses from cryo-electron micrographs. Microbiol. Mol. Biol. Rev. **63:**862–922.
2. **Belnap, D. M., B. M. McDermott Juniorperiod, D. J. Filman, N. Cheng, B. L. Trus, H. J. Zuccola, V. R. Racaniello, J. M. Hogle, and A. C. Steven.** 2000. Three-dimensional structure of poliovirus receptor bound to poliovirus. Proc. Natl. Acad. Sci. USA **97:**73–78.
3. **Bergelson, J. M., J. G. Mohanty, R. L. Crowell, N. F. St. John, D. M. Lublin, and R. W. Finberg.** 1995. Coxsackievirus B3 adapted to growth in RD cells binds to decay-accelerating factor (CD55). J. Virol. **69:**1903–1906.
4. **Bhella, D., I. G. Goodfellow, P. Roversi, Y. Chaudhry, D. J. Evans, and S. M. Lea.** 2004. The structure of echovirus type 12 bound to a two-domain fragment of its cellular attachment protein decay-accelerating factor (CD55). J. Biol. Chem. **279:**8325–8332.
5. **Brodbeck, W. G., D. Liu, J. Sperry, C. Mold, and M. E. Medof.** 1996. Localization of classical and alternative pathway regulatory activity within the decay-accelerating factor. J. Immunol. **156:**2528–2533.
6. **Chothia, C.** 1975. Structural invariants in protein folding. Nature (London) **254:**304–308.
7. **Clarkson, N. A., R. Kaufman, D. M. Lublin, T. Ward, P. A. Pipkin, P. D. MInor, D. J. Evans, and J. W. Almond.** 1995. Characterization of the echovirus 7 receptor: domains of CD55 critical for virus binding. J. Virol. **69:** 5497–5501.
8. **Collaborative Computational Project Number 4.** 1994. The CCP4 suite: programs for protein crystallography. Acta Crystallogr. D **50:**760–763.
9. **Colonno, R. J., J. H. Condra, S. Mizutani, P. L. Callahan, M. E. Davies, and M. A. Murcko.** 1988. Evidence for the direct involvement of the rhinovirus canyon in receptor binding. Proc. Natl. Acad. Sci. USA **85:**5449–5453.
10. **Curry, S., M. Chow, and J. M. Hogle.** 1996. The poliovirus 135S particle is infectious. J. Virol. **70:**7125–7131.
11. **Gauntt, C. J., M. D. Trousdale, D. R. L. Labadie, R. E. Pague, and T. Nealon.** 1979. Properties of coxsackievirus B3 variants which are amyocarditic or myocarditic for mice. J. Med. Virol. **3:**207–220.
12. **Goodfellow, I. G., R. M. Powell, T. Ward, O. B. Spiller, J. W. Almond, and D. J. Evans.** 2000. Echovirus infection of rhabdomyosarcoma cells is inhibited by antiserum to the complement control protein CD59. J. Gen. Virol. **81:**1393–1401.
13. **He, Y., P. R. Chipman, J. Howitt, C. M. Bator, M. A. Whitt, T. S. Baker, R. J. Kuhn, C. W. Anderson, P. Freimuth, and M. G. Rossmann.** 2001. Interaction of coxsackievirus B3 with the full-length coxsackievirus-adenovirus receptor. Nat. Struct. Biol. **8:**874–878.
14. **He, Y., F. Lin, P. R. Chipman, C. M. Bator, T. S. Baker, M. Shoham, R. J. Kuhn, M. E. Medof, and M. G. Rossmann.** 2002. Structure of decay-accelerating factor bound to echovirus 7: a virus-receptor complex. Proc. Natl. Acad. Sci. USA **99:**10325–10329.
15. **Hewat, E. A., E. Neumann, J. F. Conway, R. Moser, B. Ronacher, T. C. Marlovits, and D. Blaas.** 2000. The cellular receptor of human rhinovirus 2 binds around the 5-fold axis and not in the canyon: a structural view. EMBO J. **19:**6317–6325.
16. **Hofer, F., M. Gruenberger, H. Kowalski, H. Machat, M. Huettinger, E. Kuechler, and D. Blaas.** 1994. Members of the low density lipoprotein receptor family mediate cell entry of a minor-group common cold virus. Proc. Natl. Acad. Sci. USA **91:**1839–1842.

17. **Jones, T. A., J. Y. Zou, S. W. Cowan, and M. Kjeldgaard.** 1991. Improved methods for building protein models in electron density maps and the location of errors in these models. Acta Crystallogr. A **47:**110–119.
18. **Karnauchow, T. M., S. Dawe, D. M. Lublin, and K. Dimock.** 1998. Short consensus repeat domain 1 of decay-accelerating factor is required for enterovirus 70 binding. J. Virol. **72:**9380–9383.
19. **Kolatkar, P. R., J. Bella, N. H. Olson, C. M. Bator, T. S. Baker, and M. G. Rossmann.** 1999. Structural studies of two rhinovirus serotypes complexed with fragments of their cellular receptor. EMBO J. **18:**6249–6259.
20. **Kuttner-Kondo, L., D. E. Hourcade, V. E. Anderson, N. Muqim, L. Mitchell, D. C. Soares, P. N. Barlow, and M. E. Medof.** 2007. Structure-based mapping of DAF's active site residues that decay acccelerate the C3 convertases. J. Biol. Chem. **282:**18552–18562.
21. **Kuttner-Kondo, L. A., L. Mitchell, D. E. Hourcade, and M. E. Medof.** 2001. Characterization of the active sites in decay-accelerating factor. J. Immunol. **167:**2164–2171.
22. **Lea, S. M., R. M. Powell, T. McKee, D. J. Evans, D. Brown, D. I. Stuart, and P. A. van der Merwe.** 1998. Determination of the affinity and kinetic constants for the interaction between the human echovirus 11 and its cellular receptor, CD55. J. Biol. Chem. **273:**30443–30447.
23. **Lee, B., and F. M. Richards.** 1971. The interpretation of protein structures: estimation of static accessibility. J. Mol. Biol. **55:**379–400.
24. **Lindberg, A. M., R. L. Crowell, R. Zell, R. Kandolf, and U. Pettersson.** 1992. Mapping of the RD phenotype of the Nancy strain of coxsackievirus B3. Virus Res. **24:**187–196.
25. **Lukacik, P., P. Roversi, J. White, D. Esser, G. P. Smith, J. Billington, P. A. Williams, P. M. Rudd, M. R. Wormald, D. J. Harvey, M. D. Crispin, C. M. Radcliffe, R. A. Dwek, D. J. Evans, B. P. Morgan, R. A. Smith, and S. M. Lea.** 2004. Complement regulation at the molecular level: the structure of decay-accelerating factor. Proc. Natl. Acad. Sci. USA **101:**1279–1284.
26. **Martino, T. A., M. Petric, M. Brown, K. Aitken, C. J. Gauntt, C. D. Richardson, L. H. Chow, and P. P. Liu.** 1998. Cardiovirulent coxsackieviruses and the decay-accelerating factor (CD55) receptor. Virology **244:**302–314.
27. **Medof, M. E., D. M. Lublin, M. Holers, D. J. Ayers, R. R. Getty, J. F. Leykam, J. P. Atkinson, and M. L. Tykocinski.** 1987. Cloning and characterization of cDNAs encoding the complete sequence of decay-accelerating factor of human complement. Proc. Natl. Acad. Sci. USA **84:** 2007–2011.
28. **Milstone, A. M., J. Petrella, M. D. Sanchez, M. Mahmud, J. C. Whitbeck, and J. M. Bergelson.** 2005. Interaction with coxsackievirus and adenovirus receptor, but not with decay-accelerating factor (DAF), induces A-particle formation in a DAF-binding coxsackievirus B3 isolate. J. Virol. **79:**655–660.
29. **Muckelbauer, J. K., M. Kremer, I. Minor, G. Diana, F. J. Dutko, J. Groarke, D. C. Pevear, and M. G. Rossmann.** 1995. The structure of coxsackievirus B3 at 3.5 Å resolution. Structure **3:**653–667.
30. **Neumann, E., R. Moser, L. Snyers, D. Blaas, and E. A. Hewat.** 2003. A cellular receptor of human rhinovirus type 2, the very-low-density lipoprotein receptor, binds to two neighboring proteins of the viral capsid. J. Virol. **77:**8504–8511.
31. **Oliveira, M. A., R. Zhao, W. Lee, M. J. Kremer, I. Minor, R. R. Rueckert, G. D. Diana, D. C. Pevear, F. J. Dutko, M. A. McKinlay, and M. G. Rossmann.** 1993. The structure of human rhinovirus 16. Structure **1:**51–68.
32. **Olson, N. H., P. R. Kolatkar, M. A. Oliveira, R. H. Cheng, J. M. Greve, A. McClelland, T. S. Baker, and M. G. Rossmann.** 1993. Structure of a human rhinovirus complexed with its receptor molecule. Proc. Natl. Acad. Sci. USA **90:**507–511.
33. **Orthopoulos, G., K. Triantafilou, and M. Triantafilou.** 2004. Coxsackie B viruses use multiple receptors to infect human cardiac cells. J. Med. Virol. **74:**291–299.
34. **Pettersen, E. F., T. D. Goddard, C. C. Huang, G. S. Couch, D. M. Greenblatt, E. C. Meng, and T. E. Ferrin.** 2004. UCSF Chimera—a visualization system for exploratory research and analysis. J. Comput. Chem. **24:**1605–1612.
35. **Pettigrew, D. M., D. T. Williams, D. Kerrigan, D. J. Evans, S. M. Lea, and D. Bhella.** 2006. Structural and functional insights into the interaction of echoviruses and decay-accelerating factor. J. Biol. Chem. **281:**5169–5177.
36. **Powell, R. M., V. Schmitt, T. Ward, I. Goodfellow, D. J. Evans, and J. W. Almond.** 1998. Characterization of echoviruses that bind decay accelerating factor (CD55): evidence that some haemagglutinating strains use more than one cellular receptor. J. Gen. Virol. **79:**1707–1713.
37. **Powell, R. M., T. Ward, D. J. Evans, and J. W. Almond.** 1997. Interaction between echovirus 7 and its receptor, decay-accelerating factor (CD55): evidence for a secondary cellular factor in A-particle formation. J. Virol. **71:**9306–9312.
38. **Powell, R. M., T. Ward, I. Goodfellow, J. W. Almond, and D. J. Evans.** 1999. Mapping the binding domains on decay-accelerating factor (DAF) for haemagglutinating enteroviruses: implications for evolution of a DAF-binding phenotype. J. Gen. Virol. **80:**3145–3152.
39. **Rieder, E., A. E. Gorbalenya, C. Xiao, Y. He, T. S. Baker, R. J. Kuhn, M. G. Rossmann, and E. Wimmer.** 2001. Will the polio niche remain vacant? Dev. Biol. **105:**111–122.
40. **Rossmann, M. G.** 2000. Fitting atomic models into electron microscopy maps. Acta Crystallogr. D **56:**1341–1349.
41. **Rossmann, M. G., E. Arnold, J. W. Erickson, E. A. Frankenberger, J. P. Griffith, H. J. Hecht, J. E. Johnson, G. Kamer, M. Luo, A. G. Mosser, R. R. Rueckert, B. Sherry, and G. Vriend.** 1985. Structure of a human common cold virus and functional relationship to other picornaviruses. Nature (London) **317:**145–153.
42. **Rossmann, M. G., R. Bernal, and S. V. Pletnev.** 2001. Combining electron microscopic with X-ray crystallographic structures. J. Struct. Biol. **136:**190–200.
43. **Rossmann, M. G., Y. He, and R. J. Kuhn.** 2002. Picornavirus-receptor interactions. Trends Microbiol. **10:**324–331.
44. **Rossmann, M. G., and A. C. Palmenberg.** 1988. Conservation of the putative receptor attachment site in picornaviruses. Virology **164:**373–382.
45. **Rueckert, R. R.** 1990. Picornaviridae and their replication, p. 507–548. *In* B. N. Fields and D. M. Knipe (ed.), Virology, 2nd ed., vol. 1. Raven Press, New York, NY.
46. **Sanner, M. F., and A. J. S. Olson, J. C.** 1996. Reduced surface: an efficient way to compute molecular surfaces. Biopolymers **38:**305–320.
47. **Selinka, H. C., A. Wolde, A. Pasch, K. Klingel, J. J. Schnorr, J. H. Kupper, A. M. Lindberg, and R. Kandolf.** 2002. Comparative analysis of two coxsackievirus B3 strains: putative influence of virus-receptor interactions on phathogenesis. J. Med. Virol. **67:**224–233.
48. **Semler, B. L., and E. Wimmer (ed.).** 2002. Molecular biology of picornaviruses. ASM Press, Washington, DC.
49. **Shafren, D. R., R. C. Bates, M. V. Agrez, R. L. Herd, G. F. Burns, and R. D. Barry.** 1995. Coxsackieviruses B1, B3, and B5 use decay-accelerating factor as a receptor for cell attachment. J. Virol. **69:**3873–3877.
50. **Shafren, D. R., D. J. Dorahy, R. A. Ingham, G. F. Burns, and R. D. Barry.** 1997. Coxsackievirus A21 binds to decay-accelerating factor but requires intercellular adhesion molecule 1 for cell entry. J. Virol. **71:**4736–4743.
51. **Shafren, D. R., D. T. Williams, and R. D. Barry.** 1997. A decay-accelerating factor binding strain of coxsackievirus B3 requires the coxsackievirus-adenovirus receptor protein to mediate lytic infection of rhabdomyosarcoma cells. J. Virol. **71:**9844–9848.
52. **Smyth, M., T. Pettitt, A. Symonds, and J. Martin.** 2003. Identification of the pocket factors in a picornavirus. Arch. Virol. **148:**1225–1233.
53. **Spiller, O. B., I. G. Goodfellow, D. J. Evans, J. W. Almond, and B. P. Morgan.** 2000. Echoviruses and coxsackie B viruses that use human decay-accelerating factor (DAF) as a receptor do not bind the rodent analogues of DAF. J. Infect. Dis. **181:**340–343.
54. **Stanway, G., P. Joki-Korpela, and T. Hyypiä.** 2000. Human parechoviruses—biology and clinical significance. Rev. Med. Virol. **10:**57–69.
55. **Stuart, A. D., H. E. Eustace, T. A. McKee, and T. D. K. Brown.** 2002. A novel cell entry pathway for a DAF-using human enterovirus is dependent on lipid rafts. J. Virol. **76:**9307–9322.
56. **Tam, P. E.** 2006. Coxsackievirus myocarditis: interplay between virus and host in the pathogenesis of heart disease. Viral Immunol. **19:**133–146.
57. **Thompson, J. C., D. G. Higgins, and T. J. Gibson.** 1994. CLUSTAL W: improving the sensitivity of progressive multiple sequence alignment through sequence weighting, position-specific gap penalties and weight matrix choice. Nucleic Acids Res. **22:**4673–4680.
58. **Triantafilou, K., and M. Triantafilou.** 2004. Lipid-raft-dependent coxsackievirus B4 internalization and rapid targeting to the Golgi. Virology **326:** 6–19.
59. **Tuthill, T. J., D. Bubeck, D. J. Rowlands, and J. M. Hogle.** 2006. Characterization of early steps in the poliovirus infection process: receptor-decorated liposomes induce conversion of the virus to membrane-anchored entry-intermediate particles. J. Virol. **80:**172–180.
60. **Uhrinova, S., F. Lin, G. Ball, K. Bromek, D. Uhrin, M. E. Medof, and P. N. Barlow.** 2003. Solution structure of a functionally active fragment of decay-accelerating factor. Proc. Natl. Acad. Sci. USA **100:**4718–4723.
61. **Uncapher, C. R., C. M. DeWitt, and R. J. Colonno.** 1991. The major and minor group receptor families contain all but one human rhinovirus serotype. Virology **180:**814–817.
62. **Whitton, J. L., C. T. Cornell, and R. Feuer.** 2005. Host and virus determinants of picornavirus pathogenesis and tropism. Nat. Rev. Microbiol. **3:**765–776.
63. **Williams, D. T., Y. Chaudhry, I. G. Goodfellow, S. Lea, and D. J. Evans.** 2004. Interactions of decay-accelerating factor (DAF) with haemagglutinating human enteroviruses: utilizing variation in primate DAF to map virus binding sites. J. Gen. Virol. **85:**731–738.
64. **Williams, P., Y. Chaudhry, I. G. Goodfellow, J. Billington, R. Powell, O. B. Spiller, D. J. Evans, and S. M. Lea.** 2003. Mapping CD55 function. The structure of two pathogen-binding domains at 1.7 Å. J. Biol. Chem. **278:** 10691–10696.
65. **Xiao, C., and M. G. Rossmann.** 2007. Interpretation of electron density with stereographic roadmap projections. J. Struct. Biol. **158:**182–187.